Decrease in B_z prior to the dipolarization in the near-Earth plasma sheet

K. Shiokawa, Y. Miyashita, I. Shinohara, and A. Matsuoka

Abstract: We examine in detail the rapid decrease in B_z just before dipolarizations observed by the GEOTAIL satellite in the near-Earth plasma sheet at (X_{GSM}, Y_{GSM}) = (-8.3 R_E, -5.1 R_E). The observations were made using high-time-resolution data from a fluxgate magnetometer (16-Hz sample), a search-coil magnetometer (128 Hz), and an electric field antenna (64 Hz). Two dipolarizations were observed during a short time interval of 2 min. The magnetic B_z component suddenly decreased 2–4 s prior to the dipolarization. Characteristic waves with frequencies of 5–20 Hz and amplitudes of 1–3 mV/m and 5-15 nT/s were observed in the electric and magnetic field data at the time of the sudden decreases in B_z. We discuss two possible causes of the sudden decreases in B_z prior to the dipolarizations: (1) passage of a field-aligned line current associated with the substorm current wedge, and (2) explosive growth phase and subsequent disruption of the tail current caused by the observed characteristic field oscillations.

Key words: dipolarization, explosive growth phase, substorm, current disruption.

1. Introduction

Dipolarization of the tail magnetic field is an important feature at the onset of magnetospheric substorms. The dipolarization indicates a sudden decrease of the duskward tail current that prevailed during the substorm growth phase. [7] explained dipolarizations as tail current disruption due to wave turbulence in the thin current sheet. [16] and [1] explained dipolarizations as Earthward flow braking (dawnward inertia current) and subsequent pileup of northward magnetic flux transported from tail reconnection.

On the basis of magnetic field measurements made by the AMPTE/CCE satellite inside 10 R_E, [11] found the explosive growth phase, which is characterized by a rapid decrease of magnetic field elevation angles prior to the dipolarization. [21] reported similar "bipolar" structure (a decrease and then an increase) of B_z during the magnetic flux ropes associated with Earthward convective flow in the tail plasma sheet at $|X| > 14$ R_E. They explained these flux ropes as coming from the multiple reconnection X-lines in the near tail. [14] have also reported flux rope structures during nightside magnetic flux transfer events, which are probably caused by impulsive reconnection in the near-Earth plasma sheet. A statistical analysis of GEOTAIL data at $\sim$10–30 R_E by [13] shows that sharp dipolarizations tend to be preceded by a transient decrease in B_z, indicating that this is a common feature during the dipolarizations. [18] noted that about half of the 21 dipolarization events they studied show decrease in B_z prior to the dipolarization at X $\sim$10 R_E. [4] and N. Shirataka et al. (private communication, 2004) found that by introducing a guide field B_y in their three-dimensional reconnection model, a decrease in B_z occurs prior to the dipolarization due to a pileup of the B_y field at the leading edge of Earthward flow.

Received 18 May 2006.

K. Shiokawa and Y. Miyashita. Solar-Terrestrial Environment Laboratory, Nagoya University, Toyokawa 442-8507, Japan
I. Shinohara and A. Matsuoka. Institute of Space and Astronautical Sciences, Japan Aerospace Exploration Agency, Sagamihara 229-8510, Japan

In the ICS-8 presentation, we reported a detailed analysis of a sequence of rapid decreases in B_z prior to the dipolarizations, using high-time-resolution data from GEOTAIL measurements of magnetic and electric fields. We found intense 5–20 Hz waves during the events. The observed feature seems not to be the flux ropes or B_y pileups. We discuss alternative causes of these characteristic field variations in light of the substorm current wedge and tail current disruption. The full version of this work has already been published by [19].

2. Observation

GEOTAIL satellite data with high time resolution are used in this work. They consist of 16-Hz sampled magnetic field data obtained by a fluxgate magnetometer, 128-Hz sampled magnetic field fluctuations obtained by a search coil magnetometer, and 64-Hz sampled electric field data obtained by a 100-m tip-to-tip probe antenna. Plasma velocities were obtained by an electrostatic analyzer with a time resolution of 12 s and from DC electric field measurements with a time resolution of 3 s. Details of these instruments are given by [5], [22], and [10].

Figure 1 shows an 8-min interval of the dipolarization events observed by the GEOTAIL satellite, using the high time resolution data (16 Hz sampling in the DC magnetic field, 128 Hz in the AC magnetic field, and 64 Hz in the electric field). Two sequential dipolarizations can be clearly identified at 1549:40 UT and 1551:25 UT, as indicated by the vertical dashed lines. The elevation angle and B_z of the magnetic field rapidly decrease prior to these dipolarizations. B_y increases and then decreases at these events. The magnetic field intensity B does not significantly change at the first event, while it slightly increases at the dipolarization of the second event.

These dipolarizations are observed at the beginning of Earthward plasma velocity enhancements, as shown in the $V_{x,y,z}$ and $V_{\perp,x}$ panels. The thermal (P_i) and total (P_{total}) pressures decrease at or after these dipolarizations. The AC magnetic field obtained by a search coil magnetometer and the time derivative of the electric field (dE/dt) in the bottom panels show bursts of waves at the time of these dipolarization events. There

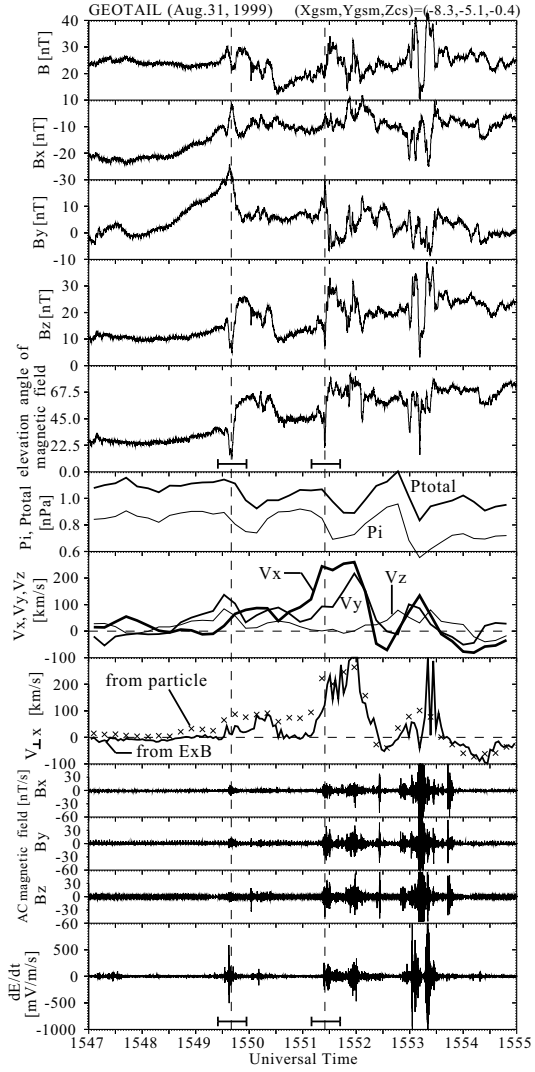

Fig. 1. From top to bottom: 16-Hz sampled B, B_x, B_y, B_z, and elevation angle (0° = tail-like, 90° = dipolar) of the magnetic field obtained by a fluxgate magnetometer, thermal pressure (P_i) and total pressure ($P_{total} = P_i + P_b$, where P_b is the magnetic pressure), V_x, V_y, and V_z obtained by the particle detector, $V_{\perp,x}$ obtained by a particle detector (crosses, 12-s resolution) and calculated from $E_y B_z / B^2$ (solid curves, 3-s resolution), 128-Hz sampled magnetic field fluctuations of B_x, B_y, and B_z, obtained by a search coil magnetometer, and the time derivative of 64-Hz sampled electric field data, obtained by GEOTAIL for an 8-min interval at 1547–1555 UT on August 31, 1999. The data are in GSM coordinates. The GEOTAIL location Z_{cs} at the top is the Z-distance from the model current sheet determined by [23]. For the $v_{\perp,x}$ calculation from the electric field data, only the E_y component is used, because GEOTAIL does not measure the E_z component. The two horizontal bars indicate the time intervals shown in Figure 2.

may be a third event at ∼1553:30 UT. Here, we focus on the first two events.

At the time in Figure 1, GEOTAIL was at (X_{GSM}, Y_{GSM}, Z_{cs}) = (-8.3, -5.1, -0.4) R_E, where Z_{cs} is the distance from the model neutral sheet as determined by [23]. Two low-latitude Pi 2 pulsations with onset times at 1526 UT and 1544 UT were observed at three Japanese ground stations in the midnight local time sector (00:26 and 00:44 LT, respectively). An auroral initial brightening was observed by the POLAR UVI imager associated with the second Pi 2 onset at 1544 UT in the dusk sector at ∼22 magnetic local time (MLT). The auroral brightening expanded toward the dawn sector, where GEOTAIL was located at 02:04 MLT at 1550 UT. The ion density, temperature, and plasma β (ratio of thermal pressure to magnetic pressure) were ∼0.5–1.0 cm^{-3}, 5–8 keV, and 2–5, respectively, at 1540–1610 UT, indicating that GEOTAIL was well within the central plasma sheet (see Figures 1 and 2 of [19]).

Figures 2a and 2b are expanded plots of the GEOTAIL data for 32-s intervals (indicated by the two horizontal bars in Figure 1) around the two dipolarizations at (a) 1549:25–1549:57 UT and (b) 1551:10–1551:42 UT. Since the electric field in the bottom panels consists of raw data from the 100-m probe antenna, 3-s spin modulation is clearly seen with some distortions due to photoelectrons ([22]).

In both Figures 2a and 2b, B_z decreases 2–4 s before the dipolarizations. B_y has peaks near the local minimum of B_z in both cases. B_x tends to decrease at the same time as B_z in Figure 2a. The total field intensity B does not significantly change in Figure 2a, while it increases coincident with the B_z increase in Figure 2b.

Intense waves are seen in both magnetic and electric field data from the beginning of the B_z decrease in Figure 2a and from ∼1 s before the B_z decrease in Figure 2b. Although the time resolution of plasma velocity is low, the Earthward convective plasma velocities in Figure 2a are rather small, less than 100 km/s, while those in Figure 2b are 100–200 km/s during the B_z decrease.

The plots in Figure 3 are a further expansion of the GEOTAIL data for 4-s intervals (indicated by the horizontal bars in Figure 2) at the beginning of the intense waves. The waves in the electric field data seem to have characteristic frequencies of 5–20 Hz and amplitudes of ∼3 mV/m in Figure 3a and ∼1-3 mV/m in Figure 3b. Waves with a similar frequency range are seen in the search-coil magnetic field data with amplitudes of ∼5 nT/s in Figure 3a and ∼15 nT/s in Figure 3b. Waves with a higher frequency range can also be seen in the search coil data, because of the higher sampling rate of 128 Hz.

3. Discussion

We observed rapid decreases in B_z 2–4 s before the dipolarizations. The event was observed two times within the 2-min interval. Convective plasma velocity was small (<100 km/s) for the first event, while it was 100-200 km/s for the second event. Characteristic waves were observed from the beginning of the decrease in B_z in both the electric and the magnetic field data. The high-time-resolution data shows that the waves have frequencies of 5–20 Hz, and large amplitudes of 1-3 mV/m in the electric field data and 5-15 nT/s in the search coil magnetic field data. The frequency of 5–20 Hz is in the range of the lower hybrid waves.

As cited in the introduction, several authors explained the decrease in B_z prior to the dipolarization as flux ropes due

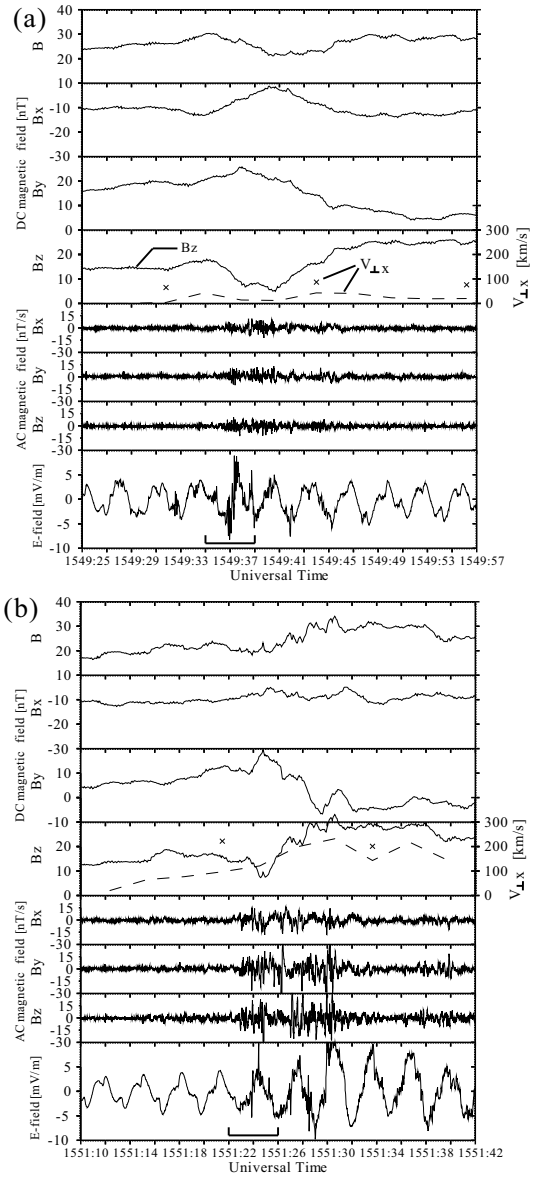

Fig. 2. From top to bottom: B, B_x, B_y, and B_z (solid curves), obtained by a fluxgate magnetometer, $v_{\perp,x}$ (crosses: from a particle detector, 12-s resolution, and dashed curves: from $E_y B_z/B^2$, 3-s resolution), AC magnetic field fluctuations of B_x, B_y, and B_z, obtained by a search coil magnetometer, and 64-Hz sampled electric field data, for 32-s intervals at (a) 1549:25–1549:57 UT and (b) 1551:10–1551:42 UT obtained by GEOTAIL on August 31, 1999. The two horizontal bars indicate the time intervals shown in Figure 3.

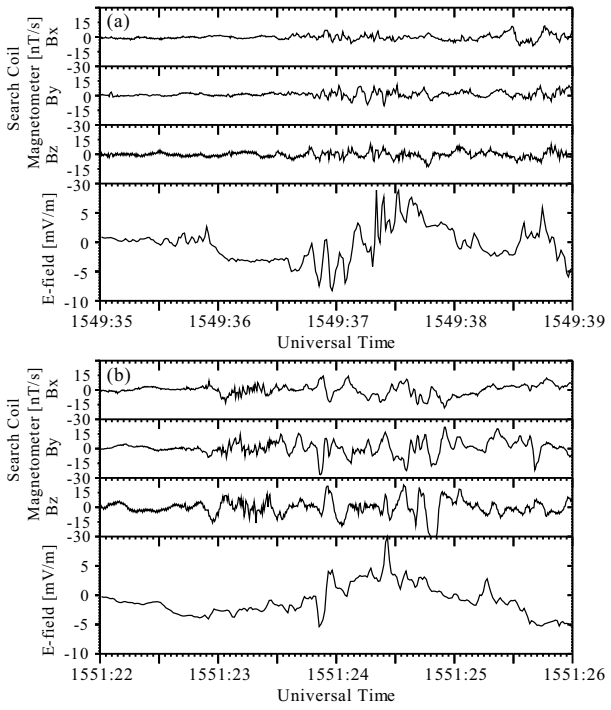

Fig. 3. 128-Hz sampled magnetic field variations obtained by a search coil magnetometer, and 64-Hz sampled electric field data, for 4-s intervals at (a) 1549:35–1549:39 UT and (b) 1551:22–1551:26 UT obtained by GEOTAIL on August 31, 1999.

to multiple/impulsive reconnection and pileup of the B_y field. The present event seems to be different from the flux ropes or pileup, because the peak in B_y is almost coincident with the local minimum of B_z and $B_z > 0$ everywhere. For flux ropes and B_y pileups, there would be a bipolar B_z with a peak in B_y near the inflection point of the B_z signature. Moreover, intense waves were observed in the lower hybrid frequency range. In this work, we would like to consider two alternative explanations for the observed decrease in B_z prior to the dipolarization.

One explanation is the passage of field-aligned line current associated with the substorm current wedge, as shown schematically in Figure 4. Because B_x was continuously negative, GEOTAIL was in the south of the tail current sheet. If GEOTAIL was above (north of) the upward field-aligned current (b) or below (south of) the downward field-aligned current (c), it would observe a decrease and then an increase in B_z, as shown in Figure 4d. B_y would have a peak when the line current is closest to the satellite. This configuration may explain the observed B_z and B_y changes in Figure 1. The model in Figure 4 predicts that the B_y peak will coincide with zero crossing of B_z. The B_y peak, however, coincides with the negative peak of B_z in Figure 2. If the field-aligned current not only aligns with GSM-X but has some component in the GSM-Y and -Z directions or if the current has some sheet structures, it may be possible to reproduce the observed B_z and B_y variations by a crossing of field-aligned currents. However, this model requires that for the present case, the field-aligned current expands quickly in longitude two times during the 2-min interval. This model also does not explain why the intense 5–20 Hz waves were observed at the start of the decrease in B_z.

The idea of field-aligned line current was first considered by [11] for the events of the explosive growth phase. They excluded this idea because the observed variation in the geomagnetically outward component of the magnetic field was opposite to that of the model in the VDH coordinate system. It is not clear whether the same logic using the VDH coordinates is applicable to the present case, since the radial distance of 10

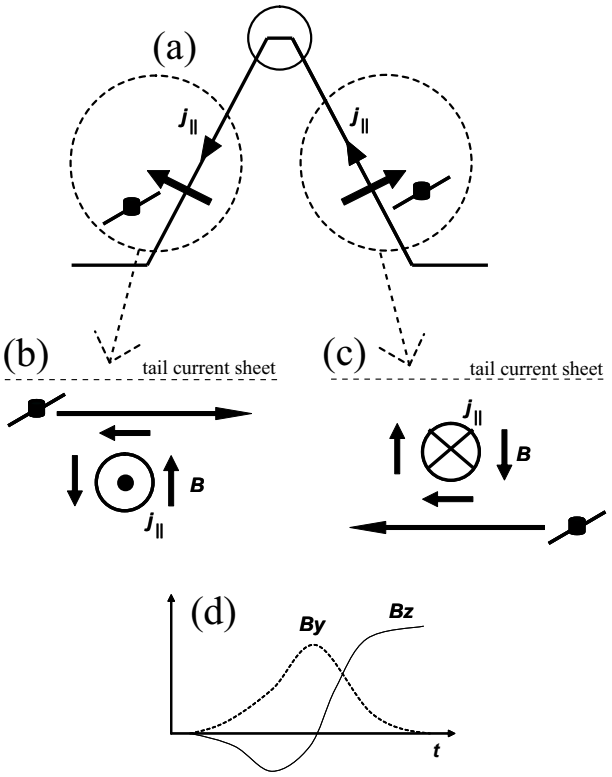

Fig. 4. Schematics of (a) the substorm current wedge, (b) and (c) two possible motions of GEOTAIL relative to the field-aligned line current (looking from the tail to Earth), which explain the observed decrease in B_z and increase in B_y prior to the dipolarization (d). Because B_x was negative throughout the event, GEOTAIL was southward of the tail current sheet.

R_E is just at the geomagnetic hinging distance, where dipole configuration changes to the tail configuration ([3]).

The other explanation for the rapid decrease in B_z prior to the dipolarization is an explosive growth phase and a localized tail current disruption, as schematically shown in Figure 5. Because B_x was continuously negative during the present event, GEOTAIL was in the south of the tail current sheet (Figure 5a). At the late growth phase, the tail current sheet can be suddenly intensified by some processes discussed below (explosive growth phase, Figure 5b). The magnetic field becomes tail-like Earthward of the current intensification region and dipolar tailward of the intensification region. This explains the sudden decrease in B_z, if the satellite was located Earthward of the current intensification region.

Then in Figure 5c, a localized current disruption occurs, as expressed by an equivalent dawnward current, possibly because of an anomalous resistivity due to the observed intense waves with frequencies of 5–20 Hz. The intense waves may be generated by the cross-tail current instability due to the sudden intensification of the tail current in Figure 5b. The magnetic field configuration just tailward of the current disruption region becomes more tail-like due to this localized current disruption. This again explains the observed decrease in B_z on a short time scale, if the satellite is located tailward of the disruption region. The disrupted current will be closed to the field-aligned current, forming a substorm current wedge.

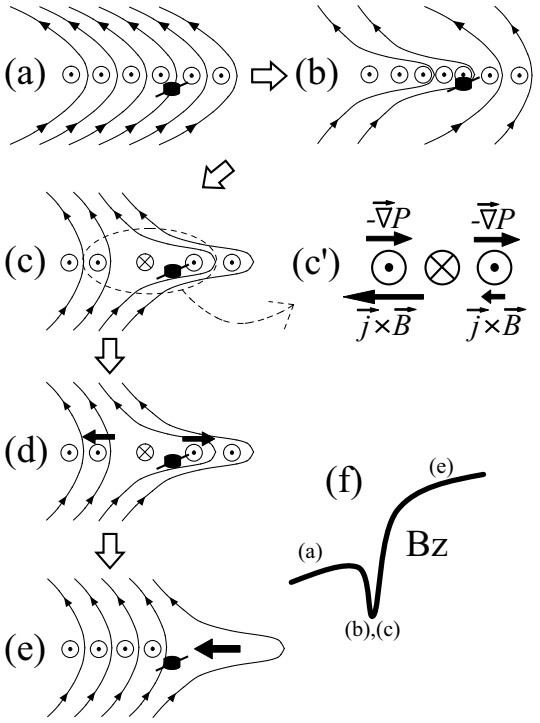

Fig. 5. Schematics (X-Z plane looking from dusk to dawn) of a sequence of explosive growth and disruption of the tail current, explaining the observed decrease in B_z prior to the dipolarization (indicated in (f)). (a) Before the event, (b) intensification of tail current (explosive growth phase), (c) localized tail current disruption (indicated as a dawnward tail current), (c') enhanced (reduced) magnetic field inside (outside) the current disruption region increases (decreases) the Earthward $\mathbf{j} \times \mathbf{B}$ force, (d) plasma tries to move Earthward (tailward) inside (outside) the current disruption region, and (e) the whole plasma moves Earthward due to a reduction in pressure gradient force, causing dipolarization (increase in B_z) on the MHD time scale. The accumulation of plasma and magnetic field may then increase the tailward pressure gradient force to stop the flow (back to (a)). Satellite location was just tailward of the current disruption region in the southern hemisphere.

The field configuration in Figure 5c is, however, unstable on an MHD time scale, which is longer than a few seconds. The current disruption (equivalent dawnward current) produces additional northward B_z Earthward of the disruption region and southward B_z tailward of the disruption region. Thus, as shown in Figure 5c', the Earthward $\mathbf{j} \times \mathbf{B}$ force becomes larger than the prevailing tailward pressure gradient force Earthward of the current disruption region, while it becomes smaller tailward of the current disruption region. As a result, plasma tends to move Earthward/tailward at Earthward/tailward of the current disruption region (Figure 5d). Since the Earthward plasma motion reduces the pressure gradient force tailward of the moving region, the whole plasma finally moves Earthward (Figure 5e). This unbalance of $\mathbf{j} \times \mathbf{B}$ force has been discussed by [8] (Section 6.6).

Because the Earthward plasma motion causes accumulation of the plasma and magnetic field inside the disruption region, the tailward pressure gradient force may increase again and the

whole plasma may stop moving (back to Figure 5a). This may explain the sequence of the present event, where dipolarizations took place twice within 2 min. The B_x and B_y changes observed at the time of the decrease in B_z may be explained if the duskward sheet current at the explosive growth phase and/or the dawnward disruption current are tilted in the $X-Y$ plane.

In the above discussion, two processes, i.e., explosive growth phase (Figure 5b) and subsequent localized current disruption (Figure 5c), are considered for the cause of the sudden decrease in B_z. For the explosive growth phase, [11] and [12] proposed that sudden intensification of the cross-tail current sheet with a time scale of $\sim$1 min can be caused by a positive feedback process between the unmagnetization of ions and the thinning of the current sheet. [2] proposed that the kinetic ballooning instability can cause explosive growth phase with a time scale (period) of 50-75 s. [6] proposed that the entropy antidiffusion by lower-hybrid drift instability can cause sudden intensification of cross-tail current sheet with a time scale of $\sim$1 min. All these possible processes of explosive growth phase predict the time scale of $\sim$1 min, which is longer than that of the present events (2-4 s). The decrease in B_z by a localized current disruption can be a time scale of a few seconds, since the current disruption is a non-MHD process, which should be relaxed on MHD time scale as shown in Figures 5c-5e. As shown in Figure 2, the intense 5-20 Hz waves were observed from the beginning of the B_z decrease. This fact also supports the idea that the waves are responsible for the current disruption that causes decrease in B_z. Anyhow, if explosive growth phase occurs prior to the current disruption to drive the thinning and intensification of the cross-tail current sheet, it would be difficult to distinguish which (explosive growth phase or current disruption) is the cause of the observed decrease in B_z.

The intense lower hybrid waves with frequencies of 5–20 Hz and amplitudes of 1–3 mV/m observed at the decrease in B_z may be responsible for the tail current disruption. Model calculations would be necessary to check whether these waves are sufficient to disrupt the tail current. Recently [20] reported similar waves at a lower hybrid frequency range ($\sim$5-16 Hz) based on the GEOTAIL observation in the tail plasma sheet at 10–13 R_E. They concluded that these waves are not likely to be the cause of the tail current disruption, because their maximum amplitude was not observed until after the start of magnetic field dipolarization and Earthward flow. They suggest that these waves are a consequence of the dynamics of the magnetotail, since they are associated with plasma flow. In the present case, the amplitude of the waves is already very high at the start of the decrease in B_z, as shown in Figures 1 and 2. Thus, the waves may be responsible for substorm initiation through cross-tail current instability. If the waves in the lower hybrid frequency range are also generated by plasma dynamics, it would be very difficult to distinguish the cause and the result based on a single satellite measurement.

The relation between the observed field variations and the Earthward plasma flow is important for verifying these models. For the first event in Figure 2a, the plasma velocity increases slightly to $\sim$100 km/s, while the second event in Figure 2b occurs when the plasma velocity increases to a few hundred km/s. This flow enhancement would be consistent with the longitudinal expansion of field-aligned line current model in Figure 4, if, for example, the substorm current wedge is driven by the braking of Earthward flow ([16] and [17]).

The decrease of the total pressure at or after the dipolarization in Figure 1 may not be not consistent to the flow braking view for the present cases. We should note that for the present events the ion energy tends to exceed the upper limit of the ion detector (40 keV), so that the pressure measurements may become ambiguous. However, this pressure reduction at the dipolarization has been reported in several literatures. [15] called the reduction of the plasma pressure associated with dipolarization and earthward bursty flow as plasma bubbles. [9] reported similar reduction of the plasma pressure in the equatorial inner plasma sheet at substorm onset, and concluded that this reduction leads to the expansion-phase reduction of cross-tail current.

The model of explosive growth and disruption of tail current (Figure 5) also predicts Earthward flow enhancement at the time of dipolarization. For the second event in Figure 2b, the flow was enhanced prior to the decrease in B_z. This may contradict the current disruption model. However, if the tail current disruption and subsequent Earthward flow occur on a different spatial scale, one could expect an overlap of Earthward flow and a decrease in B_z on a non-MHD short time scale.

In any case, the time resolutions of the plasma velocities (3 s in $\mathbf{E}\times\mathbf{B}$ and 12 s in plasma moment) are not sufficient to allow a discussion of timing in relation to field variation. Both methods have problems in the determination of plasma velocities, i.e., the electric field is reliable only for the E_y direction, and ion energy exceeds the upper limit (40 keV) of the plasma detectors for the present event. High-time-resolution measurement over a broad energy range (up to 100 keV) would be essential for plasma velocity determination in the near-Earth tail.

4. Conclusion

We have investigated a sequential dipolarization event observed by the GEOTAIL satellite in the near-Earth plasma sheet at (X_{GSM}, Y_{GSM}) = (-8.3, -5.1)R_E, using high-time-resolution data from a fluxgate magnetometer (16-Hz), a search-coil magnetometer (128 Hz), and an electric field antenna (64 Hz). The dipolarization event took place 5–7 min after ground Pi 2 onset and a POLAR UVI auroral brightening, and was observed dawnside (02 MLT) of the main onset region (22 MLT). The observed characteristics of the dipolarization are summarized as follows:

1. Two dipolarizations were observed within a 2 min interval. The magnetic field B_z suddenly decreased 2-4 s before the dipolarization in both cases.

2. Characteristic electric and magnetic field oscillations with frequencies of 5-20 Hz (lower hybrid frequency range) and amplitudes of 1-3 mV/m and 5-15 nT/s were observed coincident with the sudden decrease in B_z.

We discuss two possible causes of the sudden decrease in B_z prior to dipolarization: (1) passage of field-aligned line current associated with the substorm current wedge, and (2) explosive growth and disruption of the cross-tail current sheet. From the present observation it is difficult to distinguish which process caused the observed magnetic field features. In the former case, the observed intense waves may be a consequence

of plasma dynamics (plasma flow) during dipolarization. In the latter case, the observed waves may cause the tail current disruption. Plasma measurements with a high time resolution (higher than 1 s) would be key to differentiating between these two models.

Acknowledgments: GEOTAIL data were provided through DARTS at the Institute of Space and Astronautical Science (ISAS), Japan Aerospace Exploration Agency, Japan. K. S. is grateful to A. T. Y. Lui and T. Nagai for their helpful comments. The Principal Investigator of the Polar UVI experiment is G. K. Parks. The POLAR UVI images were supplied through the NASA MSFC home page. This work was supported by a Grant-in-Aid for Scientific Research of the Ministry of Education, Culture, Sports, Science and Technology of Japan (13640449).

References

1. Baumjohann, W., M. Hesse, S. Kokubun, T. Mukai, T. Nagai, and A. Petrukovich, Substorm dipolarization and recovery, *J. Geophys. Res., 104(A11)*, 24,995–25,000, 1999.
2. Cheng, C. Z., and A. T. Y. Lui, Kinetic ballooning instability for substorm onset and current disruption observed by AMPTE/CCE, *Geophys. Res. Lett., 25(21)*, 4091–4094, 1998.
3. Fairfield, D. H., A statistical determination of the shape and position of the geomagnetic neutral sheet, *J. Geophys. Res., 85*, 775–780, 1980.
4. Hashimoto, C., R. TanDokoro, and M. Fujimoto, Effects of guide field in three-dimensional magnetic reconnection, in *Frontiers in magnetospheric plasma physics*, edited by M. Hoshino, Y. Omura, and L. J. Lanzerotti, pp. 130–134, 2005.
5. Kokubun, S., T. Yamamoto, M. H. Acuña, K. Hayashi, K. Shiokawa, and H. Kawano, The GEOTAIL magnetic field experiment, *J. Geomag. Geoelectr., 46*, 7–21, 1994.
6. Lee, L. C., L. Zhang, A. Otto, G. S. Choe, H. J. Cai, Entropy antidiffusion instability and formation of a thin current sheet during geomagnetic substorms, *J. Geophys. Res., 103(A12)*, 29,419–29,428, 1998.
7. Lui, A. T. Y., R. E. Lopez, B. J. Anderson, K. Takahashi, L. J. Zanetti, R. W. McEntire, T. A. Potemra, D. M. Klumpar, E. M. Greene, and R. Strangeway, Current disruptions in the near-Earth neutral sheet region, *J. Geophys. Res., 97*, 1461–1480, 1992.
8. Lui, A. T. Y., P. H. Yoon, and C.-L. Chang, Quasi-linear analysis of ion Weibel instability in the Earth's neutral sheet, *J. Geophys. Res., 98*, 153–163, 1993.
9. Lyons, L. R., C.-P. Wang, T. Nagai, T. Mukai, Y. Saito, and J. C. Samson, Substorm inner plasma sheet particle reduction, *J. Geophys. Res., 108(A12)*, 1426, doi:10.1029/2003JA010177, 2003.
10. Mukai, T., S. Machida, Y. Saito, M. Hirahara, T. Terasawa, N. Kaya, T. Obara, M. Ejiri, and A. Nishida, The low energy particle (LEP) experiment onboard the GEOTAIL satellite, *J. Geomag. Geoelectr., 46*, 669–692, 1994.
11. Ohtani, S., K. Takahashi, L. J. Zanetti, T. A. Potemra, and R. W. McEntire, Initial signatures of magnetic field and energetic particle fluxes at tail reconfiguration: Explosive growth phase, *J. Geophys. Res., 97*, 19,311–19,324, 1992.
12. Ohtani, S., A. T. Y. Lui, K. Takahashi, D. G. Mitchell, and T. Sarris, Ion dynamics and tail current intensification prior to dipolarization: The June 1, 1985, event, *J. Geophys. Res., 105(A11)*, 25,233–25,246, 2000.
13. Ohtani, S., M. A. Shay, and T. Mukai, Temporal structure of the fast convective flow in the plasma sheet: Comparison between observations and two-fluid simulations, *J. Geophys. Res., 109*, A03210, doi:10.1029/2003JA010002, 2004.
14. Sergeev, V. A., R. C. Elphic, F. S. Mozer, A. Saint-Marc, and J. A. Sauvaud, A two-satellite study of nightside flux transfer events in the plasma sheet, *Planet. Space Sci., 40*, 1551–1572, 1992.
15. Sergeev, V. A., V. Angelopoulos, J. T. Gosling, C. A. Cattell, and C. T. Russell, Detection of localized, plasma-depleted flux tubes or bubbles in the midtail plasma sheet, *J. Geophys. Res., 101(A5)*, 10,817–10,826, 1996.
16. Shiokawa, K., W. Baumjohann, and G. Haerendel, Braking of high-speed flows in the near-Earth tail, *Geophys. Res. Lett., 24*, 1179–1182, 1997.
17. Shiokawa, K., et al., High-speed ion flow, substorm current wedge, and multiple Pi 2 pulsations, *J. Geophys. Res., 103*, 4491–4507, 1998.
18. Shiokawa, K., I. Shinohara, T. Mukai, H. Hayakawa, and C. Z. Cheng, Magnetic field fluctuations during substorm-associated dipolarizations in the nightside plasma sheet around $X = -10$ R_E, *J. Geophys. Res., 110*, A05212, doi:10.1029/2004JA010378, 2005a.
19. Shiokawa, K., Y. Miyashita, I. Shinohara, and A. Matsuoka, Decrease in Bz prior to the dipolarization in the near-Earth plasma sheet, J. Geophys. Res., 110, A09219, doi:10.1029/2005JA011144, 2005b.
20. Sigsbee, K., C. A. Cattell, D. Fairfield, K. Tsuruda, and S. Kokubun, Geotail observations of low-frequency waves and high-speed earthward flows during substorm onsets in the near magnetotail from 10 to 13 RE, *J. Geophys. Res., 107(A7)*, 1141, doi:10.1029/2001JA000166, 2002.
21. Slavin, J. A., R. P. Lepping, J. Gjerloev, D. H. Fairfield, M. Hesse, C. J. Owen, M. B. Moldwin, T. Nagai, A. Ieda, and T. Mukai, Geotail observations of magnetic flux ropes in the plasma sheet, *J. Geophys. Res., 108(A1)*, 1015, doi:10.1029/2002JA009557, 2003.
22. Tsuruda, K., H. Hayakawa, M. Nakamura, T. Okada, A. Matsuoka, F. S. Mozer, and R. Schmidt, Electric field measurements on the GEOTAIL satellite, *J. Geomag. Geoelectr., 46*, 693–711, 1994.
23. Tsyganenko, N. A., Modeling the Earth's magnetospheric magnetic field confined within a realistic magnetopause, *J. Geophys. Res., 100*, 5599–5612, 1995.